Devonian rise in atmospheric oxygen correlated to the radiations of terrestrial plants and large predatory fish

Tais W. Dahl[a,b,1], Emma U. Hammarlund[b,c,d], Ariel D. Anbar[e,f], David P. G. Bond[g], Benjamin C. Gill[h], Gwyneth W. Gordon[e], Andrew H. Knoll[a,h], Arne T. Nielsen[i], Niels H. Schovsbo[j], and Donald E. Canfield[b]

[a]Department of Organismic and Evolutionary Biology, Harvard University, Cambridge, MA 02138; [b]Nordic Center for Earth Evolution (NordCEE) and Institute of Biology, University of Southern Denmark, DK-5230 Odense C, Denmark; [c]Department of Palaeozoology, Swedish Museum of Natural History, Box 50007, SE-104 05 Stockholm, Sweden; [d]Department of Geological Sciences, Stockholm University, SE-106 91 Stockholm, Sweden; [e]School of Earth and Space Exploration, Arizona State University, Tempe, AZ 85287; [f]Department of Chemistry and Biochemistry, Arizona State University, Tempe, AZ 85287; [g]School of Earth and Environment, University of Leeds, LS2 9JT, UK; [h]Department of Earth and Planetary Sciences, Harvard University, Cambridge, MA 02138; [i]Natural History Museum of Denmark, DK-1350 Copenhagen K, Denmark; and [j]Geological Survey of Denmark and Greenland, DK-1350 Copenhagen K, Denmark

Contributed by Donald E. Canfield, August 17, 2010 (sent for review May 18, 2010)

The evolution of Earth's biota is intimately linked to the oxygenation of the oceans and atmosphere. We use the isotopic composition and concentration of molybdenum (Mo) in sedimentary rocks to explore this relationship. Our results indicate two episodes of global ocean oxygenation. The first coincides with the emergence of the Ediacaran fauna, including large, motile bilaterian animals, ca. 550–560 million year ago (Ma), reinforcing previous geochemical indications that Earth surface oxygenation facilitated this radiation. The second, perhaps larger, oxygenation took place around 400 Ma, well after the initial rise of animals and, therefore, suggesting that early metazoans evolved in a relatively low oxygen environment. This later oxygenation correlates with the diversification of vascular plants, which likely contributed to increased oxygenation through the enhanced burial of organic carbon in sediments. It also correlates with a pronounced radiation of large predatory fish, animals with high oxygen demand. We thereby couple the redox history of the atmosphere and oceans to major events in animal evolution.

Phanerozoic | molybdenum | black shale | ocean oxygenation | paleocean redox

The concentration of O_2 in the Earth's atmosphere and oceans has increased over time from negligible levels early in Earth history to the 21% we have in the atmosphere today (1–3). Our understanding of this history is indirect, based mainly on a series of geochemical proxies reflecting chemical interactions between O_2 and other oxidation-reduction (redox) sensitive elements. These proxies include the isotopic compositions and concentrations of elements such as S, Fe, and Mo preserved in sedimentary rocks (3–7). Several of these proxies (4, 5, 8, 9) indicate an increase in oceanic O_2 during the Ediacaran Period (635 to 542 million years ago, Ma), roughly synchronous with the emergence of large, motile bilaterian animals and, therefore, suggestive of a physiological link between Ediacaran evolution and environmental change. Despite this, the distribution of organic-rich shales (10, 11), the ratio of pyrite sulfur to organic carbon in shales (12), and modeling of the sulfur isotope record (13, 14) all indicate that large tracts of subsurface ocean remained anoxic well into the early Phanerozoic Eon (the "age of visible animals," since 542 million years ago). Levels of ocean and atmospheric oxygenation, however, are unquantified from these proxies. Indeed, the most comprehensive history of Phanerozoic oxygenation has been inferred from biogeochemical models. These models diverge, however, on their predictions for the Paleozoic, suggesting either low (15) or high levels of atmospheric oxygen (16, 17). Here, we present an independent record of ocean oxygenation history derived from the isotopic composition and concentration of Mo in black shales.

The geochemical behavior of Mo is controlled by the relative availability of dissolved H_2S and O_2 in the oceans. In oxic waters, Mo is soluble and exists as the molybdate anion, MoO_4^{2-}. In sulfidic waters, molybdate reacts with H_2S to form particle-reactive oxythiomolybdates that are readily removed from solution (see *SI Appendix* for further details). Although the sulfidic removal pathway is efficient, sulfidic environments are relatively rare today. As a result, Mo accumulates in the modern oxygenated oceans to a relatively high concentration of 105 nM [compared to rivers at 6 nM (18)], with a correspondingly long residence time of *ca.* 800 kyrs (4, 19). Because this is much longer than the ocean's mixing time (~1,500 yrs), seawater is well mixed with respect to Mo and carries a homogeneous Mo isotopic composition (20).

Mo and Fe Biogeochemistry

The isotopic composition of Mo in seawater depends on the redox chemistry of the global ocean because the major sedimentary sinks impart distinct isotope signatures. δ^{98}Mo measures the enrichment of $^{98}Mo/^{95}Mo$ in a sample relative to our in-house standard, RochMo2 (Alfa Aesar Specpure Lot# 802309E), where seawater is indistinguishable (21) from results obtained in other laboratories (18, 20, 22):

$$\delta^{98}\mathrm{Mo} = ((^{98}\mathrm{Mo}/^{95}\mathrm{Mo})/(^{98}\mathrm{Mo}/^{95}\mathrm{Mo})_{\mathrm{standard}} - 1)\cdot 1000[‰]. \quad [1]$$

Modern seawater (SW) is enriched in heavy Mo isotopes; $\delta^{98}Mo_{SW} = 2.3 \pm 0.1‰$ (20) relative to riverine and hydrothermal discharge at 0.7‰ and 0.8‰, respectively (18). This offset reflects the balance of Mo removal into three major types of sedimentary sinks. The first and second sinks include sediments deposited under oxic conditions in the deep ocean and mildly reducing water columns in shelf settings (i.e., oxygen-minimum zones), respectively. These lead to varying degrees of Mo isotope fractionation, ranging from about $2.8 \pm 0.1‰$ ($\Delta_{SW\text{-}OX}$) for deep-sea oxic removal to about $0.7 \pm 0.2‰$ ($\Delta_{SW\text{-}SAD}$) for mildly reducing settings with sulfide precipitation at depth in the sediment (SAD) (Fig. S1 and Table S2). Similar fractionations are also observed under intermittently euxinic conditions and when sulfide concentrations are low and where Mo removal is incomplete (23, 24). These Mo removal pathways are therefore grouped with the SAD sink. The third sink includes sediments deposited under persistent and strongly euxinic conditions, in which sulfide

Author contributions: T.W.D. and E.U.H. designed research; T.W.D. and E.U.H. performed research; T.W.D., E.U.H., and G.W.G. analyzed data; E.U.H., A.D.A., D.P.G.B., B.C.G., G.W.G., A.T.N., and N.H.S. contributed new reagents/analytic tools; and T.W.D., E.U.H., A.D.A., A.H.K., and D.E.C. wrote the paper.

The authors declare no conflict of interest.

Freely available online through the PNAS open access option.

[1]To whom correspondence should be addressed. E-mail: tdahl@fas.harvard.edu.

This article contains supporting information online at www.pnas.org/lookup/suppl/doi:10.1073/pnas.1011287107/-/DCSupplemental.

is present in the water column and Mo is removed quantitatively, or nearly so, resulting in little or no isotope fractionation. Such environments are rare today, but they account for a disproportionately large share of Mo removal, because the accumulation rate is 2–3 orders of magnitude higher where H_2S is present and particle-reactive oxythiomolybdates can form (24–26). Hence, Mo isotopes provide a sensitive measure of the global extent of euxinic conditions. Because greater Mo isotope fractionation is observed during the oxic removal of Mo from seawater, high seawater δ^{98}Mo values imply more oxygenated oceans, while low values imply more widespread reducing conditions and greater sulfidic Mo removal (7).

The δ^{98}Mo of ancient global oceans can be inferred from the isotopic composition of Mo in sedimentary rocks deposited under locally euxinic conditions. Sedimentary Fe speciation, in turn, can be used to constrain local depositional redox conditions (5, 27, 28). Here, we use the ratio of highly reactive to total Fe to distinguish deposition below an anoxic water column from an oxic water-column setting (i.e., $Fe_{HR}/Fe_T > 0.38$). The ratio of pyrite to highly reactive iron in anoxic settings is used to distinguish ferruginous from euxinic conditions (i.e., $Fe_P/Fe_{HR} > 0.7$). Sediments deposited under oxygenated bottom waters but with sulfidic pore waters are distinguished by $Fe_{HR}/Fe_T < 0.38$ and a Mo enrichment factor >2 times that of average crust, Mo $EF = (Mo/Al)/(Mo/Al)_{crust.} > 2$, using $(Mo/Al)_{crust} = 0.19$ ppm/wt% (29). High Mo enrichment can also be found in euxinic settings, but also with accompanying Fe_{HR} enrichment.

Mo in Ancient Rocks

In this study, we focus on samples whose Fe speciation results point to deposition in euxinic basins because these are the lithologies most likely to record the δ^{98}Mo of seawater. We compiled δ^{98}Mo, Mo, and Mo/TOC from 180 black shales (64 samples new to this study) from 25 Proterozoic and Phanerozoic marine successions (Table S1; details in *SI Appendix*). In this compilation (Fig. 1), it is immediately apparent that the heaviest δ^{98}Mo values increased during two episodes. We start with a long-lasting Proterozoic plateau of approximately 1.1‰ with a brief excursion to approximately 1.6‰ followed by a decline to intermediate values of approximately 1.4‰ in the latest Neoproterozoic (~550 Ma), and an increase to near-modern values of 2.0‰ sometime between the mid-Silurian and the mid-Devonian (~430 – 390 Ma) A relatively small further rise to modern values has occurred within the last 360 Myrs.

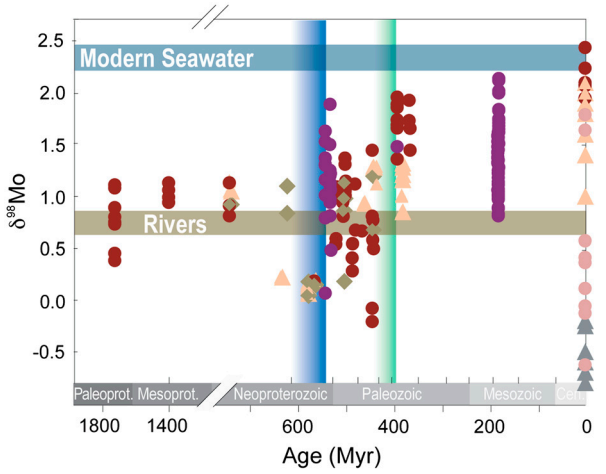

Fig. 1. Bulk δ^{98}Mo of sediments deposited in the last 1,800 million years under various redox conditions: euxinic (red circle), ferruginous (brown diamond), oxic with sulfidic sediments (sand-colored triangle), and oxic sediments with Mn-oxides (gray triangle). Data with Mo EF < 2 or Mo/Mo_{crust} < 2 are dominated by detrital material (not shown). Some published data have no local redox constraints (purple circle). Mildly or intermittently euxinic conditions (pink circle) are known to fractionate Mo isotopes in the modern system but cannot be distinguished from highly euxinic sediments in the past. The blue and green vertical lines mark the Ediacaran emergence of large animals including motile bilaterians and the Devonian invasion of vascular land plants, respectively. Typical error of the isotope determination is ±0.14‰ (2sd, standard reproducibility).

The most straightforward interpretation of these data is that they reflect secular evolution of seawater δ^{98}Mo. We note, however, that the Fe speciation proxy cannot distinguish sediments deposited in highly euxinic settings from those deposited under mildly or intermittently euxinic conditions, where Mo isotopes can be fractionated, recording δ^{98}Mo values lower than those of seawater (27). Therefore, the heaviest δ^{98}Mo values in a euxinic sedimentary sequence are those most likely to reflect seawater δ^{98}Mo. The δ^{98}Mo from any individual euxinic sedimentary succession may be offset toward lower values than true seawater due to fractionation during removal (into intermittently low sulfidic waters, for example) (24) or, perhaps, dilution with riverine discharge in hydrographically restricted basins (30). While such factors may influence individual sequences, it is unlikely they will affect only the oldest basins and govern consistent differences between time intervals (see *SI Appendix* for a statistical treatment). Therefore, we propose that our data record a two-stage increase in $\delta^{98}Mo_{SW}$, and that this indicates two major episodes of ocean oxygenation since the late Proterozoic Eon.

Mo Mass Balance Model

We explore the evolution of $\delta^{98}Mo_{SW}$ further with a simple mass balance model, where the $\delta^{98}Mo_{SW}$ of seawater is controlled by removal into the three Mo sinks described above: (*i*) deep oxic sediments (OX), (*ii*) sediments in which sulfide is present at depth (SAD; including also intermittently euxinic settings and mildly euxinic settings with low water-column sulfide concentrations), and (*iii*) euxinic (EUX) sediments. $\delta^{98}Mo_{SW}$ is modeled as a function of six parameters: (*i*) δ^{98}Mo of riverine discharge, (*ii–iv*) mean fractionation into major sinks, (*v*) the fraction of total Mo removed into highly euxinic sediments (EUX/total), with the rest buried in noneuxinic and only mildly or intermittently euxinic sediments ([SAD + OX]/total), and (*vi*) the partitioning of the noneuxinic sink into deep oxic sediments and the SAD sink (OX/[OX + SAD]). We generate steady-state solutions and keep the δ^{98}Mo of riverine discharge and the fractionations within the Mo cycle constant at modern values (details in *SI Appendix*).

Model solutions (Fig. 2) are given as trajectories of constant seawater δ^{98}Mo through solution space, reflecting variable Mo removal pathways. The model indicates that through most of the Proterozoic Eon (δ^{98}Mo = 1.1‰), Mo was preferentially removed via the euxinic pathway. Whether this removal occurred onto expansive sulfidic oxygen-minimum zones (OMZ) (31, 32) or under deep-sea sulfidic conditions (33) is unclear. Our data, however, suggest that the euxinic sink accounted for 45 to 65% of total Mo removal, corroborating earlier results (7). The deep oxic sink must have been much less important than it is today, and the remainder of the Mo was buried in noneuxinic, but sulfidic shelf sediments (perhaps under OMZs with water chemistry similar to today's, where oxygen-free, but nonsulfidic water conditions are found), or under mildly or intermittently sulfidic water-column conditions. Our model cannot distinguish these two possibilities, because, as pointed out above, each produces a similar isotope fractionation.

The increase in δ^{98}Mo to 1.4‰ during the late Ediacaran Period is consistent with an increase in the deep ocean oxic Mo sink or an increase of the SAD sink at the expense of the euxinic sink, or both. If sulfidic OMZ waters made up a large component of the Mesoproterozoic euxinic sink, then a reduction of these in favor of more modern, generally sulfide-free OMZs could also explain the increase in δ^{98}Mo to 1.4‰. There is independent evidence for oxic deep basins in the late Ediacaran

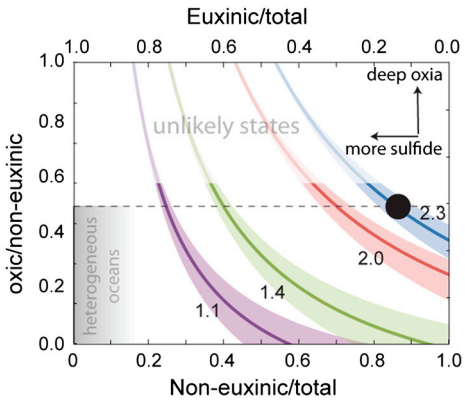

Fig. 2. Model results showing how seawater δ^{98}Mo responds to Mo burial into its different sinks (model details in *SI Appendix*). Contours show range of solutions for a given seawater δ^{98}Mo that represents modern seawater (2.3‰), early Devonian seawater (2.0‰), early Paleozoic seawater (1.4‰), and Mesoproterozoic seawater (1.1‰). The black circle represents modern state (Table S3). The shaded area at bottom left represents states where the sulfidic sinks are dominant, so that the ocean becomes heterogeneous in dissolved molybdenum. The faded area at top lacks the intermediate redox sink, despite the extreme end-members (OX and EUX) being substantial (top). Both regions are considered unlikely.

(5, 9) suggesting that Mo removal through the oxic pathway with Mn-oxides was already in place in deep ocean settings. However, the persistently low δ^{98}Mo and Mo/TOC values imply that the sulfidic pathways continued to dominate Mo removal well into the early Paleozoic Eon, if not in the water column then just below the sediment–water interface.

Our model results further show that the increase in δ^{98}Mo to 2.0‰ from the Silurian into the Devonian Period strictly requires a substantial deepwater oxic Mo sink more intense than in earlier oceans. This is because only the deepwater oxic sink imposes a fractionation large enough to allow the $\delta^{98}Mo_{sw}$ to exceed the river input value by 1.3‰, as observed in the mid-Devonian and younger shales. Extensive black shale deposition (11, 27) suggests that the euxinic sink remained substantial in Late Devonian seaways; nonetheless, Mo isotopes in these shales indicate persistent expansion of the deep-water oxic sink.

Mo Concentrations Through Time

Mo is removed with organic matter into black shales; hence, the ratio of molybdenum to total organic carbon (TOC), Mo/TOC, also relates to the extent of ocean oxygenation (Fig. 3). According to previous discussions (4), the concentration of Mo in overlying seawater is roughly reflected in the Mo/TOC of organic-rich shales. At constant riverine discharge, the increasing proportion of Mo removal into the oxic sink implies that the other sinks became smaller. Contraction of areas with rapid Mo accumulation would cause an increase in seawater Mo concentration ($[Mo]_{SW}$). Broadly speaking, the greater the sulfidic sink for Mo, the lower the concentration of seawater Mo and the lower the Mo/TOC ratio in euxinic shales (with considerable variability). Therefore, observed patterns of increase in both average and maximal Mo/TOC in black shales (Fig. 3) are both coincident and consistent with the Mo isotope evidence for a two-stage increase in ocean oxygenation.

Apparently short-lived positive excursions of Mo/TOC and δ^{98}Mo near the Precambrian–Cambrian boundary are suggestive of a more complex pattern of secular variation, and this warrants further attention.

Implications for Biological Evolution

Our compilation of Mo isotopic and elemental abundance data is based on a proxy that is inferred to be well-mixed in the ocean (details in *SI Appendix*). It thus reflects a global ocean redox history defining two episodes of ocean oxygenation since the late

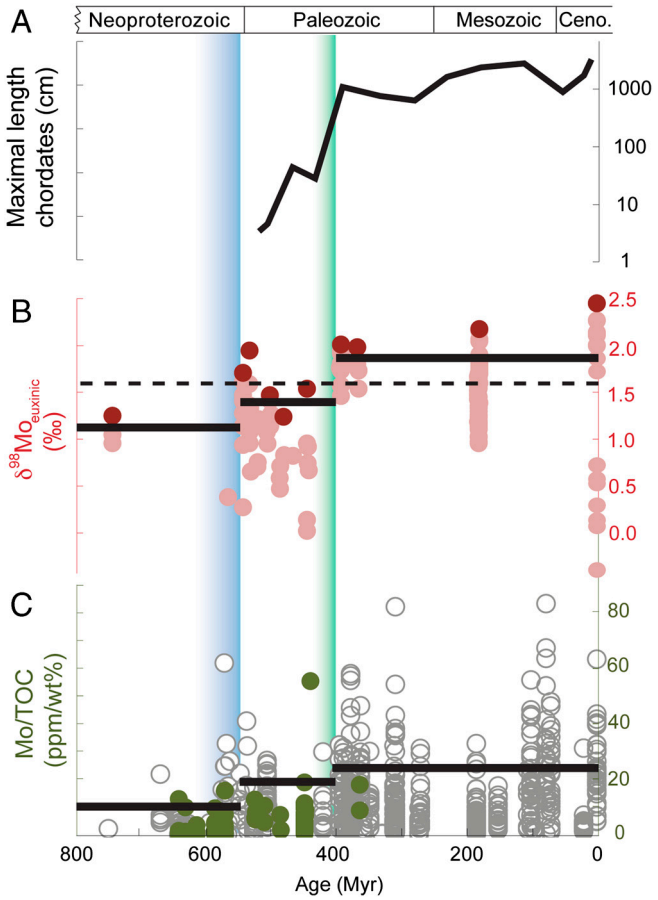

Fig. 3. (*A*) Size maxima of vertebrates is used as a measure of maximal specific metabolic rate at a given time (42). (*B*) $\delta^{98}Mo_{SW}$ euxinic samples over the last 800 Ma with seawater value inferred from highly euxinic sediments (red circles) and mildly euxinic sediments fractionated to lower values (pink circles). Seawater values above the dashed line require a substantial oxic Mo sink. (*C*) Mo/TOC of black shales (new data, solid green circles; old data, gray circles; compilation summarized in SI Appendix). In *B* and *C* solid lines represent 90% percentiles for the three time periods: 800-542 Ma, 541-390 Ma, and 390-0 Ma. These three time periods are distinct from each other; see statistical analysis in *SI Appendix*. The Ediacaran emergence of large animals and the Devonian invasion of vascular land plants are shown by graded column bars in blue and green, respectively.

Neoproterozoic. The first is consistent with other lines of geochemical evidence (4, 5, 8, 9), demonstrating that Mo isotopic data capture a significant redox event originally inferred from independent geochemical data. This event also correlates with the initial diversification of large animals, including motile bilaterian species thriving in shallow waters (e.g., *Kimberella*) (34). Our data suggest, however, that even after this event, the oceans remained far less oxygenated than today, because the persistently more widespread sulfidic environments in early Paleozoic oceans would be difficult to sustain for 150 million years by ocean stagnation alone at near-modern oxygen levels. The physiological pO_2 requirement for Cambrian animals inferred by comparison to modern relatives is >ca. 0.1 PAL (present atmospheric level) (35), corresponding to the level where benthic mass mortality is observed in modern settings (15–30 μM) (36). This provides a minimum value for pO_2 in the Early Paleozoic atmosphere and surface ocean. Oxygen levels, however, may not have been much higher than this. Thus, the long standing view that late Neoproterozoic events increased pO_2 from about 10–15% PAL to something more like modern levels (2, 37) is best retired in favor of one in which oxygen increased from Proterozoic levels just a

few percent of today's (e.g., ref. 31) to levels perhaps 15–50% PAL (Fig. S7).

The second Devonian event has received much less attention (14) but might, in absolute terms, have been the greatest oxygenation in Earth history. This oxygenation, moreover, correlates with both the diversification of vascular plants (38) and the expansion of large predatory fish (39), both events of major biological significance. Existing models of Phanerozoic atmospheric history differ with respect to oxygen levels proposed for the early Paleozoic atmosphere and oceans: Berner's Geocarb-models (17) propose relatively high pO_2 (near-modern values), whereas Bergman et al.'s COPSE model (15) predicts relatively low oxygen levels (20–60% PAL) in the early Paleozoic. Despite these differences, both predict a Devonian oxygen increase in pO_2 (15, 40), reflecting the radiation of vascular plants. This radiation accelerated land erosion enhancing global sedimentation rates, the hydrological cycle (speeding up ground water/atmosphere exchange), and promoted the burial of refractory plant material (e.g., lignin, wood). Over long time scales, a persistent increase in organic carbon burial rates and atmospheric pO_2 levels can be sustained even at constant erosion and uplift rates, because the terrestrial biomass have an approximately fourfold higher C/P than marine organic matter (e.g., lignin, cellulose, and other refractory organic compounds) (15). Enhanced burial of terrestrial organic matter acts as an O_2 source to the atmosphere. Thus, the storage of a larger organic carbon pool stabilized the atmosphere at a higher oxygen concentration state, forever altering our planet's redox history (17). Our molybdenum isotope and concentration proxies provide previously undescribed direct support for this model, identifying the beginning of a mid-Paleozoic oxygen enrichment.

Known as "the age of fishes" because of the pronounced radiation of large, jaw-bearing fish (41), the Devonian Period witnessed a dramatic increase in the maximum size of marine vertebrates (Fig. 3) (42), as well as the evolution of ammonoid cephalopods, and, more generally, a marked increase in the proportional diversity of "high energy" predators (41). Fish are among the marine animals least tolerant toward hypoxia (43), and in living fish, oxygen demand scales with size (44). Cambrian fish, known from whole-body fossils mainly from the Chengjiang deposits in China, are *ca.* 2.5–3.0 cm long, whereas well preserved Ordovician and Silurian fish reach lengths of a few tens of centimeters. Many teleost fish of similar dimensions can survive at oxygen levels below 20% PAL. However, the Devonian appearance of fish greater than 1 meter long (41) likely required more than approximately 100 μM O_2, in surface seawater, equivalent to approximately 40% PAL (see correlation between size and oxygen demand in fish in Fig. S7). Bambach (39) proposed that Devonian predator evolution reflected an expanded base of the trophic pyramid driven by phosphate-rich runoff from plant-covered continents, which potentiated increased size and/or motility in marine animals. Our geochemical results provide a complementary explanation consistent with available physiological data (41) that the expansion of predators with high metabolic rates reflects increased oxygenation of the biosphere.

Conclusions

The isotopic composition and abundance of seawater molybdenum provide measures of global ocean oxygenation, and our study shows that molybdenum-based proxies can track changes in atmospheric O_2 levels during the Phanerozoic. High abundances and δ^{98}Mo values are found in modern oxic oceans, whereas low concentrations and little or no fractionation results when Mo is preferentially removed under sulfidic conditions. The latter conditions were notably more widespread in the Proterozoic and early Paleozoic. The δ^{98}Mo and Mo/TOC of sediments deposited in anoxic and sulfidic basins display trends consistent with two major episodes of oxygenation over the last 600 million years. The first, in the late Ediacaran Period, is consistent with other geochemical indicators and correlates with the initial evolution of motile, bilaterian animals. This expansion of animal function and the subsequent radiation of diverse bilaterian animals during the so-called "Cambrian explosion," occurred at oxygen levels much lower than today's. Renewed oxygenation in the Early Devonian correlates with the initial diversification of vascular plants and may well be causally related to this event through enhanced burial of organic carbon leading to irreversible surface oxygenation. Our modeling shows most persuasively that the rise of δ^{98}Mo around 400 Ma demands, for the first time in Earth history, substantial oxic Mo removal and a persistent retreat of anoxic and sulfidic waters. Stratigraphic correlation suggests that one consequence of increased oxygen availability was the expansion of larger vertebrates with high metabolic requirements, and in particular the evolution of large predatory fish. Continued development of the paleoenvironmental proxies discussed here will yield its greatest dividends when coupled with physiologically interpretable events recorded by fossils and ocean models that can provide quantitative constraints on environmental history.

Methods

Trace metal concentrations and Mo isotope ratios were measured at the W. M. Keck Laboratory at Arizona State University on a Thermo X-series ICPMS and Thermo Neptune MC-ICPMS, respectively. Precision and accuracy of the concentration analyses are <1% and <5%. The latter is measured by repeated analyses of a certified USGS rock standard (SDO-1).

Mo isotope ratios were obtained after correction for instrumental mass bias. This was done either by external element spiking with Zr and standard-sample bracketing techniques or by doping samples with a ^{97}Mo-^{100}Mo "double spike". Quality controls for both techniques are described in ref. 24. Both methods produce δ^{98}Mo values with good reproducibility. The USGS rock standard, SDO-1, is measured to $\delta^{98}\text{Mo} = 1.13 \pm 0.07$‰ (2 s.d., 9 sessions) with the double spike method in excellent agreement with the result obtained by Zr-doping: 1.14 ± 0.14‰, 2 s.d. 65 sessions) (24).

Fe speciation analyses were performed in four steps that define a geochemically highly reactive iron pool, Fe_{HR}, including Fe-carbonate, ferric oxides, magnetite, and iron sulfides (45). The first three iron species are extracted in a sequence with acetate, dithionite, and oxalate, respectively, and quantified by atomic adsorption spectroscopy. Accuracy is evaluated by simultaneously extracting standard PACS-2, and Fe-carbonate, ferric oxides and magnetite fall within 2 s.d. of the mean ($n \leq 16$). Pyrite is extracted by chromium reduction (46), which recovers more than 90% of the inorganic sulfur (47). PACS-2 contained 0.71 ± 0.2 wt% pyrite, which is indistinguishable from previous retrieval in our lab: 0.72 ± 0.05 wt% (2 s.d., $n = 8$ sessions). The sulfur compounds were trapped in silver nitrate, forming silver sulfide, Ag_2S. This residue is used to quantify pyrite content, as 2 mol of Ag_2S corresponds to 1 mol of pyritic iron, FeS_2. Total Fe concentrations were for most samples obtained by leaching in 6 M for 96 h (48), and quantified by atomic adsorption spectroscopy. In some samples total Fe was also determined by X-ray fluorescence. Precision for all three extractions is high, since one measurement can be reproduced five times with standard deviation <0.01 wt%.

Total organic carbon (TOC) analyses were performed using a Carlo Erba Instruments CHN EA 1108 analyzer calibrated with the appropriate standards. Carbonate carbon was removed by treatment of weighed, powdered samples with 1 M HCl prior to analysis.

ACKNOWLEDGMENTS. We thank Jürgen Shieber, Remus Lazar, Sarah Gabbott, David Rudkin, and Jean-Bernard Caron for samples, and Tim Lenton, David Beerling, and Derek Vance for constructive reviews. This work was supported by Danish National Research Foundation (NordCEE), Danish Council for Independent Research (T.W.D.), the Swedish Research Council (E.H.), the NASA Astrobiology Insitute (A.H.K. and A.D.A.) and NASA Exobiology Program (A.D.A.).

1. Cloud P (1973) Paleoecological significance of banded iron-formation (Translated from English). *Econ Geol* 68(7):1135–1143 (in English).

2. Holland H (2006) The oxygenation of the atmosphere and oceans. *Philos T R Soc B* 361(1470):903–915.

3. Rouxel OJ, Bekker A, Edwards KJ (2005) Iron isotope constraints on the Archean and Paleoproterozoic ocean redox state. (Translated from English). *Science* 307(5712): 1088–1091 (in English).
4. Scott C, et al. (2008) Tracing the stepwise oxygenation of the Proterozoic ocean. *Nature* 452(7186):456–459.
5. Canfield DE, et al. (2008) Ferruginous conditions dominated later neoproterozoic deep-water chemistry (Translated from English). *Science* 321(5891):949–952 (in English).
6. Farquhar J, Bao HM, Thiemens M (2000) Atmospheric influence of Earth's earliest sulfur cycle. *Science* 289(5480):756–758.
7. Arnold GL, Anbar AD, Barling J, Lyons TW (2004) Molybdenum isotope evidence for widespread anoxia in mid-proterozoic oceans. *Science* 304(5667):87–90.
8. Fike DA, Grotzinger JP, Pratt LM, Summons RE (2006) Oxidation of the Ediacaran Ocean (Translated from English). *Nature* 444(7120):744–747 (in English).
9. Canfield DE, Poulton SW, Narbonne GM (2007) Late-Neoproterozoic deep-ocean oxygenation and the rise of animal life (Translated from English). *Science* 315(5808):92–95 (in English).
10. Leggett JK (1980) British Lower Palaeozoic black shales and their palaeo-oceanographic significance. *J Geol Soc* 137(2):139–156.
11. Berry W, Wilde P (1978) Progressive ventilation of the oceans; an explanation for the distribution of the lower Paleozoic black shales. *Am J Sci* 278(3):257–275.
12. Raiswell R, Berner RA (1986) Pyrite and organic-matter in Phanerozoic normal marine shales (Translated from English). *Geochim Cosmochim Ac* 50(9):1967–1976 (in English).
13. Berner R, Raiswell R (1983) Burial of organic carbon and pyrite sulfur in sediments over Phanerozoic time: A new theory. *Geochim Cosmochim Ac* 47:855–862.
14. Gill BC, Lyons TW, Saltzman MR (2007) Parallel, high-resolution carbon and sulfur isotope records of the evolving Paleozoic marine sulfur reservoir (Translated from English). *Palaeogeogr Palaeocl* 256(3–4):156–173 (in English).
15. Bergman NM, Lenton TM, Watson AJ (2004) COPSE: A new model of biogeochemical cycling over Phanerozoic time (Translated from English). *Am J Sci* 304(5):397–437 (in English).
16. Garrels RM, Lerman A (1984) Coupling of the sedimentary sulfur and carbon cycles; an improved model. *Am J Sci* 284(9):989–1007.
17. Berner RA (2009) Phanerozoic atmospheric oxygen: New results using the geocarbsulf model (Translated from English). *Am J Sci* 309(7):603–606 (in English).
18. Archer C, Vance D (2008) The isotopic signature of the global riverine molybdenum flux and anoxia in the ancient oceans (Translated from English). *Nat Geosci* 1(9): 597–600 (in English).
19. Morford JL, Emerson S (1999) The geochemistry of redox sensitive trace metals in sediments. *Geochim Cosmochim Ac* 63(11–12):1735–1750.
20. Siebert C, Nagler TF, von Blanckenburg F, Kramers JD (2003) Molybdenum isotope records as a potential new proxy for paleoceanography. *Earth Planet Sc Lett* 211(1–2):159–171.
21. Barling J, Arnold GL, Anbar AD (2001) Natural mass-dependent variations in the isotopic composition of molybdenum. *Earth Planet Sc Lett* 193(3–4):447–457.
22. Nakagawa Y, et al. (2008) Precise isotopic analysis of Mo in seawater using multiple collector-inductively coupled mass spectrometry coupled with a chelating resin column preconcentration method (Translated from English). *Anal Chem* 80(23): 9213–9219 (in English).
23. Neubert N, Nagler TF, Bottcher ME (2008) Sulfidity controls molybdenum isotope fractionation into euxinic sediments: Evidence from the modern Black Sea (Translated from English). *Geology* 36(10):775–778 (in English).
24. Dahl TW, et al. (2010) The behavior of molybdenum and its isotopes across the chemocline and in the sediments of sulfidic Lake Cadagno, Switzerland (Translated from English). *Geochim Cosmochim Ac* 74(1):144–163 (in English).
25. Erickson BE, Helz GR (2000) Molybdenum(VI) speciation in sulfidic waters: Stability and lability of thiomolybdates. *Geochim Cosmochim Ac* 64(7):1149–1158.
26. Zheng Y, Anderson RF, van Geen A, Kuwabara J (2000) Authigenic molybdenum formation in marine sediments: A link to pore water sulfide in the Santa Barbara Basin (Translated from English). *Geochim Cosmochim Ac* 64(24):4165–4178 (in English).
27. Gordon G, et al. (2009) When do black shales tell molybdenum isotope tales? *Geology* 37(6):535–538.
28. Lyons T, Anbar A, Severmann S, Scott C, Gill B (2009) Tracking euxinia in the ancient ocean: A multiproxy perspective and proterozoic case study. *Annu Rev Earth Pl Sc* 37:507–534.
29. Taylor SR, McLennan SM (1995) The geochemical evolution of the continental-crust (Translated from English). *Rev Geophys* 33(2):241–265 (in English).
30. McArthur J, Algeo T, van de Schootbrugge B, Li Q, Howarth R (2008) Basinal restriction, black shales, Re-Os dating, and the Early Toarcian (Jurassic) oceanic anoxic event. *Paleoceanography* 23(4):PA4217.
31. Johnston DT, et al. (2010) An emerging picture of Neoproterozoic ocean chemistry: Insight from the Chuar Group, Grand Canyon, USA. *Earth Planet Sc Lett* 290:64–73.
32. Li C, et al. (2010) A stratified redox model for the Ediacaran Ocean. *Science* 328(5974):80–83.
33. Canfield DE (1998) A new model for Proterozoic ocean chemistry. *Nature* 396(6710):450–453.
34. Fedonkin MA, Waggoner BM (1997) The Late Precambrian fossil Kimberella is a mollusc-like bilaterian organism (Translated from English). *Nature* 388(6645): 868–871 (in English).
35. Rhoads DC, Morse JW (1971) Evolutionary and ecologic significance of oxygen-deficient marine basins (Translated from English). *Lethaia* 4(4):413–428 (in English).
36. Diaz RJ, Rosenberg R (1995) Marine benthic hypoxia: A review of its ecological effects and the behavioural responses of benthic macrofauna. *Oceanography and Marine Biology—an Annual Review*, Oceanography and Marine Biology (UCL Press Ltd, London), Vol 33, pp 245–303.
37. Lyons TW, Reinhard CT, Scott C (2009) Redox redux (Translated from English). *Geobiology* 7(5):489–494 (in English).
38. Gensel PG (2008) The earliest land plants (Translated from English). *Annu Rev Ecol Evol S* 39:459–477 (in English).
39. Bambach RK (2002) Supporting predators: Changes in the global ecosystem inferred from changes in predator diversity. *The Fossil Record of Predation. Paleontological Society Papers*, eds M Kowalewski, PH Kelley, and P Dodson 8:319–352.
40. Berner R (2006) GEOCARBSULF: A combined model for Phanerozoic atmospheric O_2 and CO_2. *Geochim Cosmochim Ac* 70(23):5653–5664.
41. Bambach R (1999) Energetics in the global marinefauna: A connection between terrestrial diversification and change in the marine biosphere. *Geobios* 32(2): 131–144.
42. Payne J, et al. (2009) Two-phase increase in the maximum size of life over 3.5 billion years reflects biological innovation and environmental opportunity. *Proc Nat Acad Sci USA* 106(1):24–27.
43. Vaquer-Sunyer R, Duarte C (2008) Thresholds of hypoxia for marine biodiversity. *Proc Nat Acad Sci USA* 105(40):15452–15457.
44. Gray J, Wu R, Or Y (2002) Effects of hypoxia and organic enrichment on the coastal marine environment. *Mar Ecol Prog Ser* 238:249–279.
45. Poulton SW, Canfield DE (2005) Development of a sequential extraction procedure for iron: Implications for iron partitioning in continentally derived particulates (Translated from English). *Chem Geol* 214(3–4):209–221 (in English).
46. Zhabina NN, Volkov II (1978) *A Method of Determination of Various Sulfur Compounds in Sea Sediments and Rocks* (Ann Arbor Science Publishers, Mich), pp 735–745.
47. Wieder RK, Lang GE, Granus VA (1985) An evaluation of wet chemical methods for quantifying sulfur fractions in fresh-water wetland peat (Translated from English). *Limnol Oceanogr* 30(5):1109–1115 (in English).
48. Aller RC, Mackin JE, Cox RT (1986) Diagenesis of Fe and Si in Amazon inner shelf muds—Apparent dominance of Fe reduction and implications for the genesis of ironstones (Translated from English). *Cont Shelf Res* 6(1–2):263–289 (in English).